

Cite this article as: Lv Xueyan, Wu Shaojie, Zhou Xiaofeng, et al. Microstructure and Mechanical Properties of Hot Continuous Rolling Ti-Al-Nb-Zr-Mo Titanium Alloy Seamless Tube Welded by EBW[J]. Rare Metal Materials and Engineering, 2022, 51(12): 4376-4384.

ARTICLE

Microstructure and Mechanical Properties of Hot Continuous Rolling Ti-Al-Nb-Zr-Mo Titanium Alloy Seamless Tube Welded by EBW

Lv Xueyan¹, Wu Shaojie^{1,2}, Zhou Xiaofeng¹, Fan Limin¹, Feng Jing¹, Cheng Fangjie^{1,2}

¹School of Materials Science and Engineering, Tianjin University, Tianjin 300072, China; ²Tianjin Key Laboratory of Advanced Joining Technology, Tianjin 300072, China

Abstract: Electron beam welding (EBW) was applied to an 8-mm-thick new type Ti-Al-Nb-Zr-Mo titanium alloy seamless tube produced by hot continuous rolling. The microstructure and mechanical properties of welded joint were investigated. Results show that the base metal (BM) consists of primary α , transformed β and Widmanstatten structure. For the EBW joint, the fusion zone (FZ) consists of acicular α' , block α and Widmanstatten structure, and the size of acicular α' decreases gradually from top to bottom of the FZ. Moreover, only primary α and acicular α' form in the heat affected zone (HAZ). The average microhardness in welded joint is ranked as follows: FZ>HAZ>BM, and the microhardness of the HAZ decreases gradually from the FZ to the BM side. The joint's tensile strength is 893 MPa and the fracture occurs at the base metal. The elongation of tensile specimens can reach 10%. The impact energy of FZ reaches ~80% of that of BM and the bending specimens are bended to 180° without cracks.

Key words: titanium alloy; electron beam welding; microstructure; mechanical properties

Titanium alloy is an important metal material developed in the mid-20th century which has excellent properties including high strength, low density and superior corrosion resistance. So titanium alloy has become the preferred material in aerospace, petrochemical, ocean engineering and other fields^[1-4]. Furthermore, titanium alloy tube has also become an ideal material to replace stainless steel and copper alloy tube, which not only significantly improves the service life, but also achieves weight reduction. In particular, the titanium alloy seamless tube with high strength and corrosion resistance has a tremendous potential in oil production equipment and large ships.

At present, most titanium alloy tubes that are produced by cold rolling have the characteristics of low strength and low alloying because of the unsatisfying microstructure. As compared with the traditional cold rolling, hot continuous rolling is a simple and efficient production technology, which can realize continuous production and improve the stability of product performance, especially suitable for producing high-

strength titanium alloy seamless tube. In addition, the microstructure of titanium alloy can be precisely modified by controlling the parameters including the rolling temperature and reduction. Such modified microstructure results in good mechanical properties of titanium alloy^[5]. The titanium alloy processed by hot rolling has been extensively studied and widely reported with regard to its mechanical properties and microstructure evolution. Warwick et al^[6] found that the α phase globalization in TC4 alloy are detected when hot rolled at 950 °C, and the increased deformation degree leads to more pronounced globalization fraction, which can improve the tensile properties. Li et al^[7] found that a lamellar Widmanstatten structure forms in Ti60 near- α titanium alloy sheet when rolled in the range of β single phase temperature field. When rolled in the range of $\alpha+\beta$ two-phase temperature field, the equiaxed microstructure is formed.

The traditional titanium alloy tubes are mainly processed by welding, which is characterized by short production cycle and uniform wall thickness. However, titanium alloy has the

Received date: January 03, 2022

Foundation item: Tianjin Science and Technology Plan Project, China (18ZXJMTG00140)

Corresponding author: Cheng Fangjie, Ph. D., Professor, School of Materials Science and Engineering, Tianjin University, Tianjin 300072, P. R. China, E-mail: chfj@tju.edu.cn

Copyright © 2022, Northwest Institute for Nonferrous Metal Research. Published by Science Press. All rights reserved.

characteristics of high melting point and poor thermal conductivity, which will lead to coarse grains of welded joints. And the high-temperature β may transform to unstable acicular α' because the cooling rate is very fast, which leads to the decrease in plasticity and toughness, making it a poor performance area and not suitable for key components with high performance requirements. Therefore, titanium alloy seamless tube should be preferred for parts with high performance requirements. Titanium alloy seamless tube can not only achieve continuous and stable production, but also possess uniform performance of tubes which can reduce transmission resistance, improve corrosion resistance and increase the service life of equipment, making it suitable for ship pipeline system with high performance requirements^[8]. Compared with the titanium alloy sheet in the traditional alloy system, the microstructure of the new Ti-Al-Nb-Zr-Mo seamless tube is characterized by grain boundary α and Widmanstatten structure due to insufficient deformation and high heating temperature during hot rolling. Therefore, it is significant to study the weldability of the titanium alloy seamless tube. Electron beam welding (EBW) has been proposed as an appropriate method to join titanium alloy due to its high degree of vacuum, high energy density, fast weld speed and good weld quality^[9,10]. Many researchers have studied the microstructure and properties of titanium alloy welded by EBW. Gao et al^[11] investigated the EBW of 94-mm-thick Ti6321 alloy. The strength of the fusion zone is equivalent to that of the base metal, and the average tensile strength reach as high as 890 MPa for the welded joints. Su et al^[12] studied the EBW of 30-mm-thick TA1 titanium alloy sheets, and the surface of TA1 joint is well formed without obvious defects. The tensile strength of joint is 344 MPa, which is higher relative to that of the BM. Wang et al^[13] discovered that the tensile strength of TC11 EBW joint is close to that of the base metal, and the impact toughness is better than that of the base metal. Yang et al^[14] discovered that the EBW joint of 14-mm-thick TC4 titanium alloy mostly consists of martensite α' . The martensite α' significantly enhances the characteristics of the welded joints including its tensile strength.

Thus far, most researches on EBW of titanium alloy have been focused on the titanium sheets. There are hardly any reports about the weldability of titanium alloy seamless tube. Due to the impact of hot continuous rolling process on the microstructure, the welding process is different from that of conventional titanium sheets. In this study, a new type Ti-Al-Nb-Zr-Mo titanium alloy seamless tube produced by hot continuous rolling was welded by EBW. The microstructure and mechanical properties of the welded joint were investigated and tested.

1 Experiment

1.1 Materials

A new type of hot continuous rolling Ti-Al-Nb-Zr-Mo titanium seamless tube was used as the base metal. The titanium seamless tube had an outer diameter of 89 mm, and a

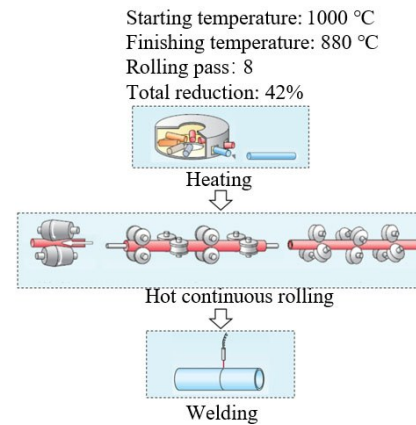


Fig.1 Hot continuous rolling process of titanium alloy seamless tube

thickness of 8 mm. The hot continuous rolling process and its parameters are illustrated in Fig. 1. The tubes were heated at 720 °C for 1 h to eliminate the residual stress after hot rolling. Table 1 lists the compositions of the BM. It is a new composition tailored for the characteristic of hot continuous rolling process. The titanium alloy of α -type exhibits desired thermal strength and weldability while the $\alpha+\beta$ type features the toughness and plasticity^[15,16]. The strength of this titanium alloy is improved obviously due to the solid solution strengthening of alloying element. Meanwhile, the toughness and plasticity of the titanium alloy are improved due to the absence of supersaturated structure.

As shown in Fig. 2a, the base metal matrix consists of α phase and β phase, which is a typical near- α titanium alloy because the content of α phase is significantly higher than that of β phase. Because the deformation of titanium alloy seamless tube in hot continuous rolling is minimal in each rolling pass while the operating temperature is relatively high, more coarse Widmanstatten structure and grain boundary α phase appear in the base metal, which is apparently different from the structure of the titanium alloy sheet. The Widmanstatten structure has higher creep resistance and fracture toughness but its plasticity is very low. As shown in Fig. 2b, the transformed β (secondary α and residual β) is surrounded by the primary α . The comparison of mechanical properties with other near- α titanium alloys is shown in Table 2^[17,18]. It can be seen that the new type of titanium alloy has overall superior mechanical properties.

1.2 Experimental preparation

The ZD-VEBW-150-30-55 high voltage vacuum electron beam welder was used in the experiment. The EBW parameters for a welded joint are listed in Table 3. The surfaces of tubes were cleaned to eliminate oxides and contaminants before welding. The electron beam welding process is divided into two steps: the first bead welding is to obtain a full penetration weld by larger beam current; secondly the

Table 1 Chemical composition of base metal (wt%)

Al	Nb	Zr	Mo	Na	Fe	V	W	Ti
2.32	1.68	1.27	0.54	0.07	0.03	0.03	0.01	Bal.

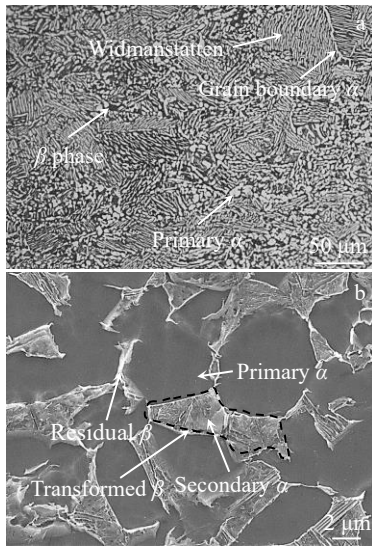


Fig.2 Microstructures of BM: (a) 200X and (b) 5000X

Table 2 Comparison of mechanical properties of near-α titanium alloys^[17,18]

Alloy	Tensile strength/MPa	Yield strength/MPa	Elongation/%	Composition
Ti75	725	585	14	Ti-3Al-2Mo-2Zr
Ti70	760	610	20	Ti-Al-Zr-Fe
BM	885	780	14	Ti-Al-Nb-Zr-Mo

Table 3 EBW parameters for welding joints

Welding process	Welding voltage/kV	Beam current/mA	Focus current/mA	Welding speed/mm·min ⁻¹
First bead	120	30	2090	800
Modification	120	16	2050	800

modification welding is used to remelt the surface with smaller beam current to partially fill the collapse of the first weld and to improve the surface appearance without affecting the performance of fusion zone, as shown in Fig.3.

1.3 Microstructure observation

The microstructure of the weld joint and the fracture surface was characterized by Olympus GX51 optical microscope (OM) and JSM-7800 scanning electron microscope (SEM). All the metallographic samples were carefully ground by 2500-grit paper and etched by the Kroll’s solution (2 mL

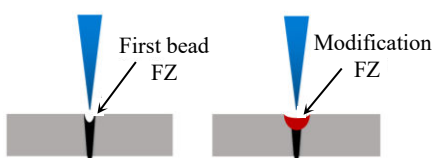


Fig.3 Schematic of first bead welding and modification welding

HF, 6 mL HNO₃, 50 mL H₂O) for about 10 s at room temperature. The Image J software was used to measure the grain size by an imaging process program.

1.4 Mechanical properties tests

The mechanical properties of the joint are evaluated with respect to the tensile strength, Charpy impact energy, bending test and microhardness. The sample sizes are shown in Fig.4. An MTS tensile testing machine was used to measure the room-temperature tensile strength. The loading rate for the test was 2 mm/min. The ZBC2752-ED pendulum impact testing machine was employed for the Charpy impact toughness. Three impact samples were taken from the FZ, HAZ and BM. The samples were kept at -10 °C for 15 min before impact test. The bending test was conducted on the front bending specimen by MTS universal electronic testing machine. Microhardness was tested by an HVA-10A automatic Vickers hardness tester using a 1 kg indenter along three lines (step length 0.5 mm) of 1, 4 and 7 mm below the front surface for 15 s.

2 Results

2.1 Microstructural characterization

2.1.1 Macrostructure of welded joint

As shown in Fig.5a, the welded joint is well formed without obvious deformation. It can be observed that the surface is silver white, which indicates that the welded joint is not oxidized. The metallograph of weld joint is shown in Fig.5b, in which four regions of different microstructures can be distinguished, marked by ①~④. The region ① is the FZ; and the HAZ is divided into two regions: the secondary HAZ as region ② and the primary HAZ as region ③; the region ④ is the BM. The profile of FZ is like a nail shape, and the FZ consists of coarse columnar grains grown symmetrically and equiaxed grains in the center. With the increase of depth, the size of columnar grains decreases. To describe the evolutions of the microstructures in FZ and HAZ clearly, the joint is divided into three layers from top to bottom, as shown in Fig.5c.

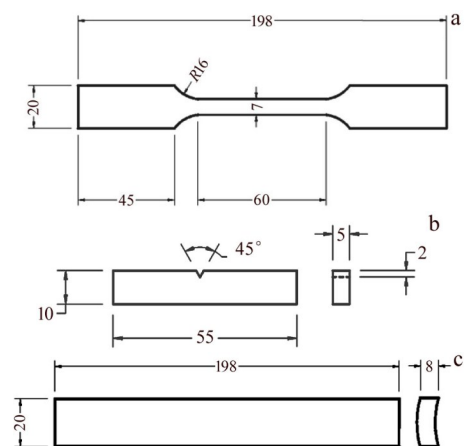


Fig.4 Schematic diagram of samples: (a) tensile sample, (b) Charpy impact sample, and (c) bending sample

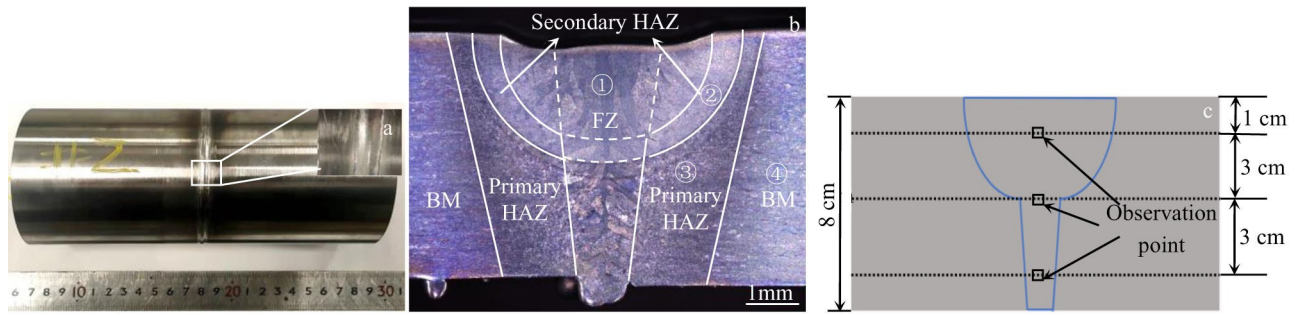


Fig.5 Microstructures of the weld bead: (a) surface morphology, (b) weld joint, and (c) schematic diagram of different layers

2.1.2 Microstructure of fusion zone

The macroscopic morphology of the fusion zone is shown in Fig.6. The microstructure of FZ varies remarkably, which shows the coarse β columnar grains. As shown in Fig.6b, the microstructure of FZ is mainly dominated by the acicular martensite α' . Moreover, the α phase nucleates at the grain boundary of the β columnar grain and transforms into the grain boundary α phase during the cooling process. In particular, part of acicular α' precipitates around the grain boundary, forming the Widmanstatten growing into the grain interior. In addition, some blocky α also exists in the β columnar grain because of the gradual slowing of cooling rate. The microstructure of the junction of modification FZ and first bead FZ is shown in Fig.6c. The modification FZ has coarser acicular α and acicular α' than first bead FZ due to larger heat input. The junction of FZ and secondary HAZ is shown in Fig.6d, and it can be seen that compared with the microstructure of modification FZ, more lamellar α exists in the secondary HAZ due to the lower peak temperature and cooling rate.

The microstructure of the FZ along the depth direction is

shown in Fig.7. Three observation points are shown in Fig.5c. The phases of different layers in the FZ consist of acicular α' , lamellar α and Widmanstatten. The size of acicular α' is different from top layer to bottom layer due to different heat input, and their size decreases along the direction of penetration. The microstructure of the bottom layer of FZ is shown in Fig.7c, and due to the less heat input and faster cooling rate of the bottom layer, the acicular α' is fine and regular in distribution as compared with the top and middle layer, which is a typical basket-like structure. As illustrated in Fig.8, the acicular martensite α' sizes of different layers are measured. The size of acicular α' at the top, middle and bottom is about 0.63, 0.60 and 0.44 μm , respectively, decreased by 30% from top to bottom.

2.1.3 Microstructure of primary HAZ and secondary HAZ

The microstructure morphologies of different positions in the primary HAZ are shown in Fig.9. Due to different heat input and cooling rates at different locations, the primary HAZ can be divided into three regions: the HAZ near FZ, the middle HAZ and the HAZ near BM. As shown in Fig.9a, predominant acicular α' and minor primary α can be observed

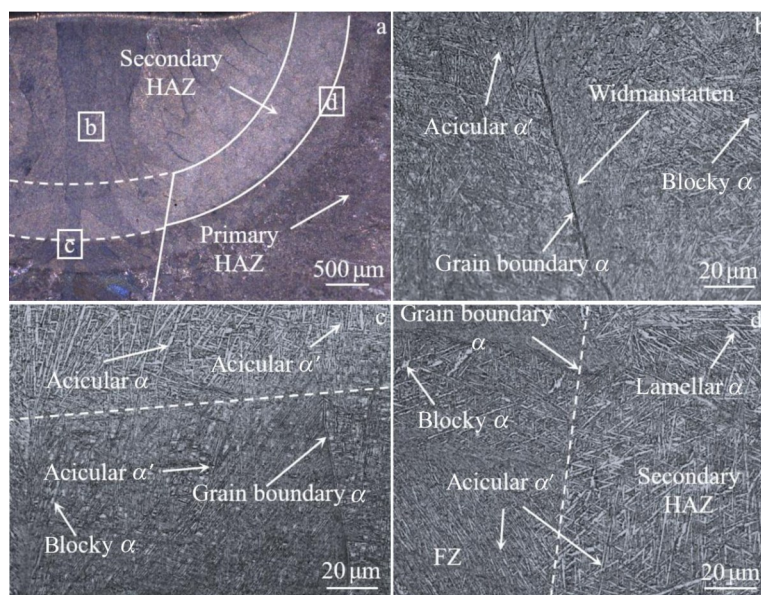


Fig.6 Microstructure morphologies of FZ (a), column grain (b), junction of modification FZ and first bead FZ (c), and junction of FZ and HAZ (d)

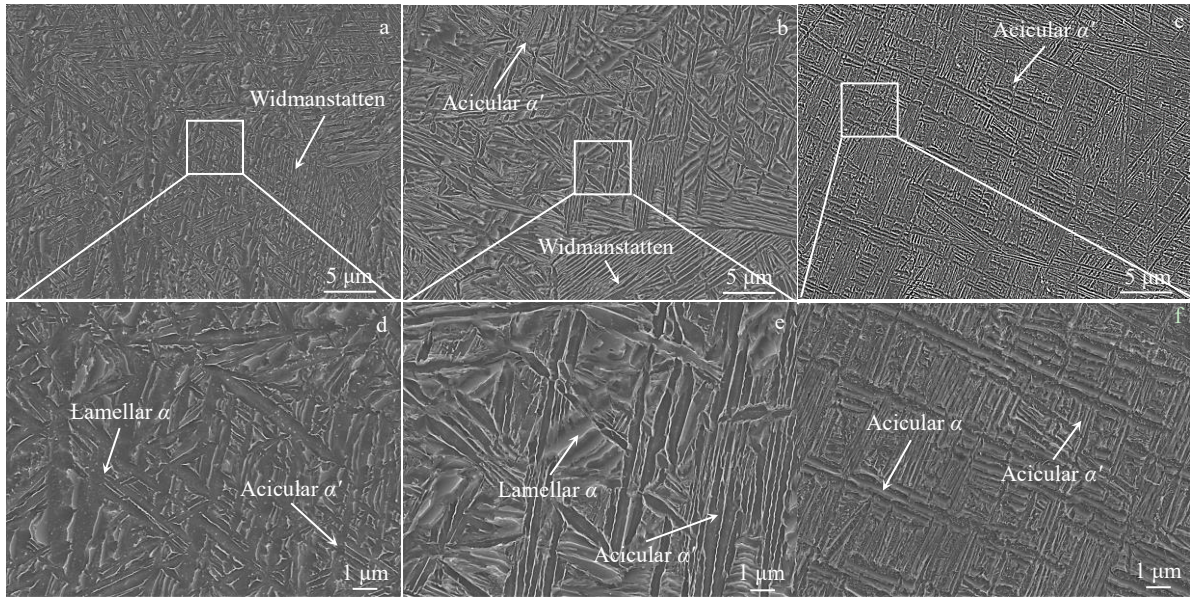


Fig.7 Microstructures of FZ along the depth direction: (a, d) top layer, (b, e) middle layer, and (c, f) bottom layer

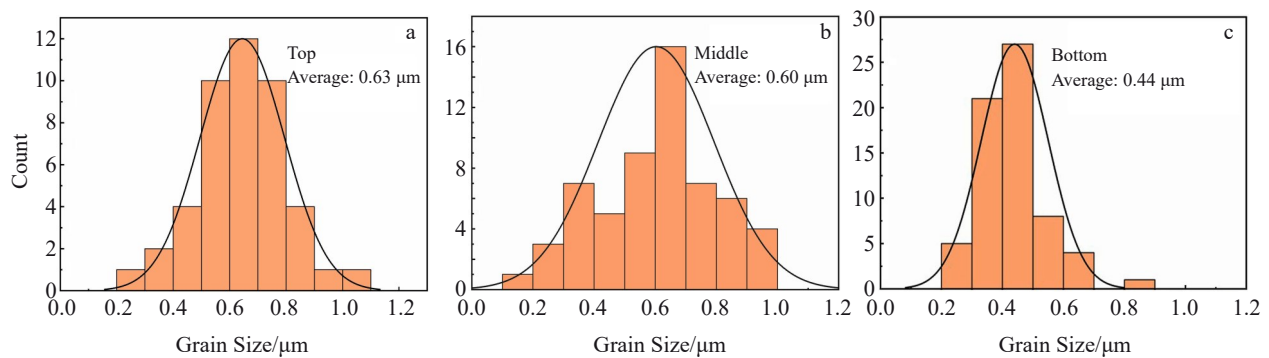


Fig.8 Grain size distribution of FZ along the depth direction: (a) top layer, (b) middle layer, and (c) bottom layer

in the HAZ near FZ. The grain boundary of primary α is blurry, and the acicular α' is distributed around the primary α . As shown in Fig.9b, the middle HAZ is composed of primary α and acicular α' , which is dependent on the peak temperature and cooling rate during welding. As shown in Fig.9c, with further away from the FZ center, the HAZ near BM is composed of a large amount of primary α and minor acicular α' . Compared with the HAZ near FZ, the size of primary α is larger and the grain boundary of primary α is clearer.

The secondary HAZ is formed in the welded joint due to the heat effect of modification welding, as shown in Fig.10a. The primary and secondary α transform into β equiaxed grains during the heat process. As can be seen in Fig.10b, the β equiaxed grains mainly consist of acicular α' and lamellar α . Because the heat input and cooling rate of the modification welding is relatively low, the high-temperature β is mostly transformed by diffusion into lamellar α rather than acicular martensite α' . The size of equiaxed grains is about 150 μm .

2.2 Mechanical properties

2.2.1 Microhardness

The positions and results of the EBW joint microhardness

measurement are shown in Fig.11. The microhardness distribution of top, middle and bottom layer in welder joint is the same, and their values have no great difference, which all increase from the BM (~ 3008.6 MPa) to the FZ (~ 3508.4 MPa). It is because the microhardness of component phase in titanium alloy is in the order of $\alpha' > \alpha > \beta$. The FZ has the highest microhardness because of the largest amount of acicular α' martensite and the microhardness of the HAZ decreases gradually in the near FZ side due to the decrease of acicular α' martensite. However, there is a rapidly fall in the HAZ near to the BM side, since the amount of acicular α' near the BM decreases sharply. Besides, because there are more acicular α' martensite in the secondary HAZ, the micro-hardness of secondary HAZ is higher than that of primary HAZ.

2.2.2 Tensile and bending properties

The average tensile properties of joints and BM are listed in Table 4. The tensile strength, yield strength, and elongation of the joint reach 893.3 MPa, 750 MPa, and 10.45%, respectively. As shown in Fig.12, all the tensile failures of the samples occur in the BM, indicating that the FZ has higher strength than BM, but the plasticity of BM is better than FZ.

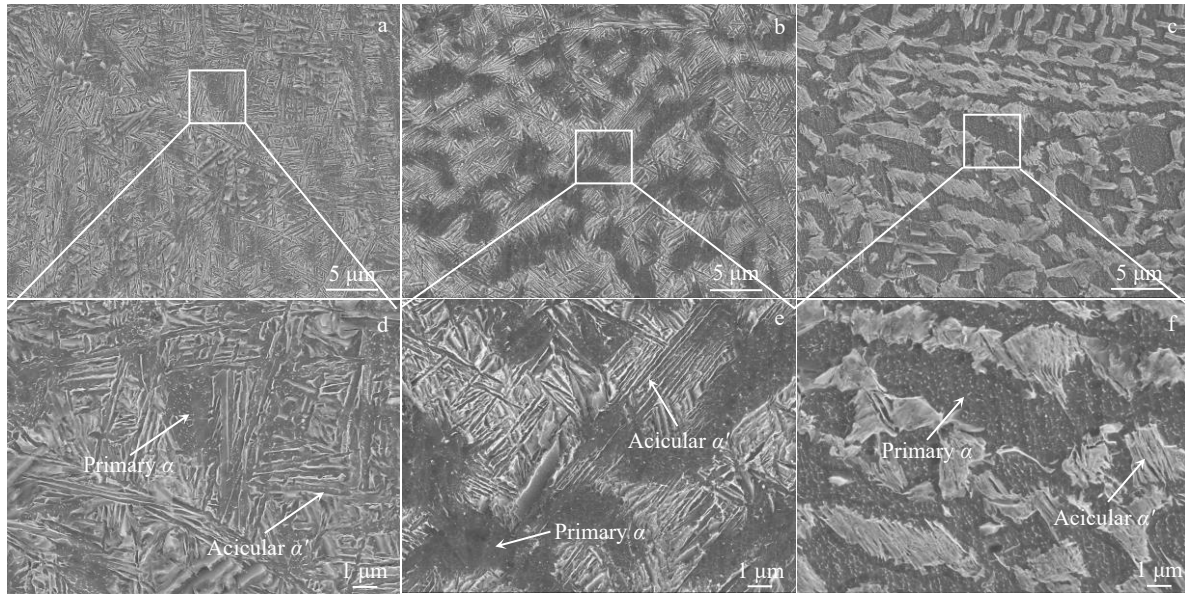


Fig.9 Microstructures of primary HAZ: (a, d) HAZ near FZ, (b, e) middle HAZ, and (c, f) HAZ near BM

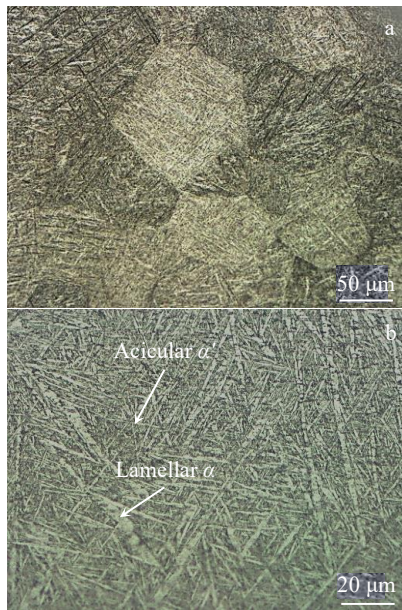


Fig.10 Microstructures of equiaxed grains of secondary HAZ

As shown in Fig.12, there are a large number of dimples in the fracture morphology of tensile specimen, and it presents ductile fracture characteristics obviously.

The higher strength of the FZ than that of the BM can be explained by the amount of acicular martensite α' . Lots of acicular martensite α' is distributed in the FZ, which is a strong barrier to the expansion of the slip band. The slip length is equal to the width of a single martensite lath, so the slip length decreases greatly, resulting in the increase in the strength [19]. In addition, this acicular martensite α' structure also decreases the plasticity of the welded joint.

The bending tests are also conducted and the bending angles of the EBW specimens are all able to reach 180° with-

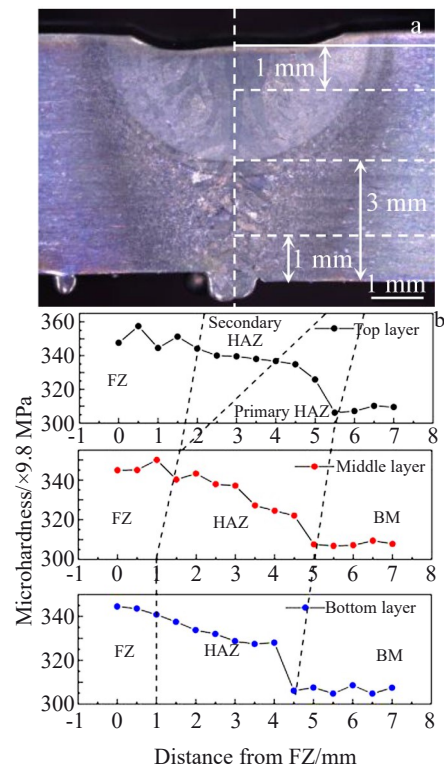


Fig.11 Microhardness distribution in the weld joint: (a) schematic diagram of microhardness measurement position and (b) results of microhardness measurement

Table 4 Tensile properties of the welded joint

Location	Tensile strength/MPa	Yield strength/MPa	Elongation/%	Fracture position
Joint	893.3	750	10.45	BM
BM	882	797	14	BM

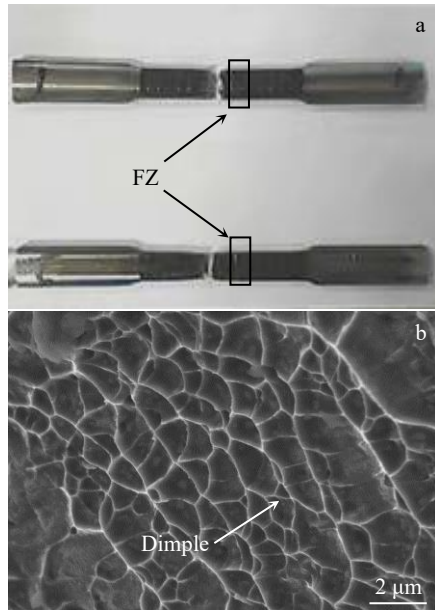


Fig.12 Tensile samples after test (a) and fracture morphology (b)

out crack. The size of acicular martensite α' in the FZ is relatively fine, which improves the bending property of welded joint to a certain extent. It can be indicated that the welded joint has good bending property and no obvious softening zone. The welded joint can carry greater bending stress.

2.2.3 Charpy impact properties

The average Charpy impact energy is shown in Table 5, and the Charpy impact energy is ranked in descending order as: BM, HAZ, and FZ, which indicates that the existence of acicular martensite α' decreases the impact toughness. The impact energy of FZ reaches $\sim 80\%$ of that of BM.

The difference of impact energy of welded joints is due to the difference of impact energy between acicular martensite α' and primary α . The impact energy consists of crack initiation energy and propagation energy. The crack propagation energy of acicular martensite α' phase is higher than that of primary α , indicating that the crack does not easily pass through staggered acicular martensite α' phase. However, the crack initiation energy of acicular martensite α' phase is lower than that of the primary α . In general, the impact energy of acicular martensite α' is lower than that of the primary α phase, indicating that the impact toughness of FZ and HAZ is lower than that of the BM^[20]. In addition, the grain size of FZ is larger than that of BM and HAZ, which also decreases the toughness of FZ.

3 Discussion

3.1 Microstructure evolution of FZ

The microstructure transformation of the titanium alloy

Table 5 Charpy impact energy of the welded joint (J)

FZ	HAZ	BM
42.7	47.8	54.3

joint is mainly related to the microstructure of base metal and the welding thermal cycle, especially the peak temperature and cooling rate. Because the EBW method has the characteristics of operating at extremely high peak temperature (2200°C) and very fast cooling rates, the microstructure evolution of the EBW joint is also different with other welding methods^[21]. In this work, the cooling curve of the welding process can be indicated as the red line annotated by " V " in Fig.13 while the curves labeled by " V_1, V_2, V_3 " represent the critical cooling rates of different microstructures obtained from the same peak temperature. At first, the base metal will be melted completely and the original microstructure will transfer into liquid phase. Then the liquid phase is cooled from peak temperature to the β phase transition point, and the high-temperature β phase nucleates and grows into coarse β columnar grain from the solid-liquid interface, as illustrated in Fig.13b. Because of the poor heat conductivity of titanium alloy, the cooling rate begins to decrease gradually with the decrease in temperature. Because the cooling rate still exceeds the critical cooling rate ($V > V_1$) in the temperature range $[T_1, T_2]$, the diffusion transformation of $\beta \rightarrow \alpha$ has no enough time to complete. So the high-temperature β is mostly transformed into the acicular α' by non-diffusion transformation. When the cooling speed is less than the critical cooling rate ($V_1 > V > V_2$) in the temperature range $[T_2, T_3]$, the high-temperature β starts to transform into blocky α by atom diffusion, which is retained in the β columnar grain. Moreover, the α phase nucleates on the original β grain boundary and transforms into the grain boundary α . The acicular α' also nucleates on the grain boundary, which leads to Widmanstatten growing to the interior of

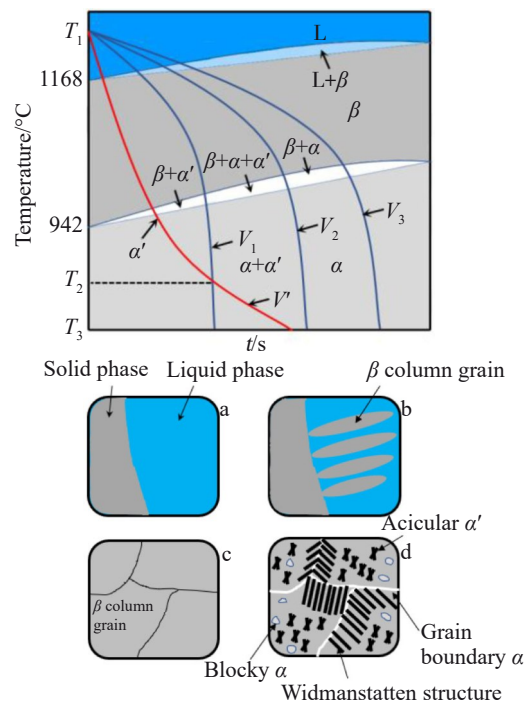


Fig.13 Schematic of microstructure evolution in FZ: (a) L, (b) L+ β , (c) β , and (d) α

the grain, as illustrated in Fig.13d.

3.2 Microstructure evolution of primary HAZ and secondary HAZ

As illustrated in Fig.14, due to different distances from the FZ, different locations of the primary HAZ experience different welding thermal cycles. The peak temperature and cooling rate decrease with increasing distance from the FZ. As can be seen from the microstructure transformation phenomenon, the sequence of transition to high temperature β phase during heating process follows: residual β , secondary α , and primary α ^[22]. At the peak temperature of the HAZ, the transformed β (secondary α and residual β) almost completely transforms into the high-temperature β , so the difference of primary HAZ at different locations is the amount of primary α phase and acicular α' .

For the HAZ near BM, the peak temperature is reached in the $(\alpha+\beta)$ temperature region, only a small fraction of primary α is transformed into the high-temperature β while the rest is retained, and then the high-temperature β transforms into acicular α' in the cooling process, as illustrated in Fig.14a. For the middle HAZ, part of primary α transforms into the high-temperature β when the peak temperature exceeds the $\alpha \rightarrow \beta$ phase transition temperature, and then transforms to acicular α' phase after a rapid cooling, as illustrated in Fig.14b. For the HAZ near FZ, the peak temperature is much higher in the β

region, and most primary α undergoes $\alpha \rightarrow \beta$ phase transition while only a few primary α phase is retained. And the high-temperature β is almost completely transformed into acicular α' phase at cooling rate higher than the critical cooling rate, as illustrated in Fig.14c. In general, as the temperature gradually decreases along the distance away from the FZ, the transformation tendency of acicular α' phase is also gradually declined^[22,23].

The modification welding process has a certain influence on the microstructure of welded joint, forming the secondary HAZ which has undergone two solid phase transitions. The peak temperature of the first thermal cycle almost reaches the liquid phase zone, and the transformed β and most primary α of the base metal transform into high-temperature β during the first thermal cycle, and then the high-temperature β transforms into the acicular α' at a rapid cooling rate. After cooling, the microstructure consists of acicular α' and a small amount of primary α . Since the parameters of the modification welding are matched with those of the first beam welding, the heat input of the modification welding is reduced accordingly^[24]. The modification welding reheats the primary HAZ near the FZ, which is similar to the tempering effect^[25]. Because the α' martensite is a non-equilibrium phase, the modification welding process will promote part of the α' martensite to transform into more lamellar α , so the secondary HAZ consists of acicular α' and lamellar α , as illustrated in Fig.14d.

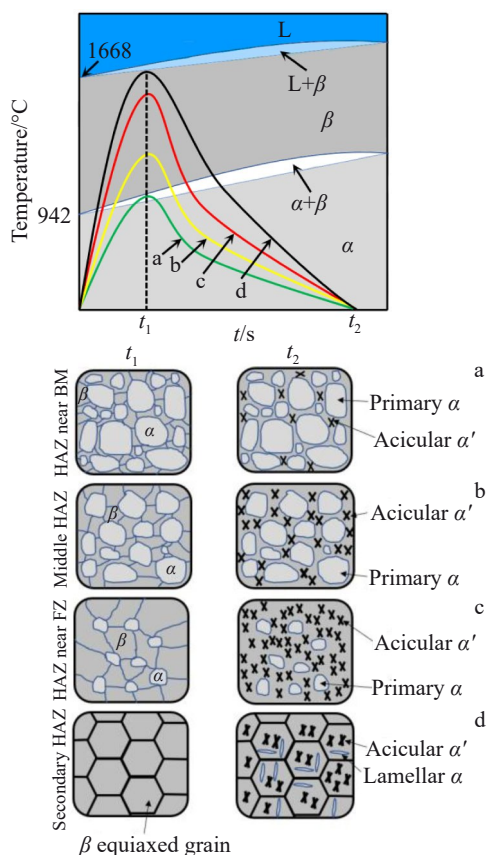


Fig.14 Schematic of microstructure evolution in primary HAZ and secondary HAZ: (a) HAZ near BM, (b) middle HAZ, (c) HAZ near FZ, and (d) secondary HAZ

4 Conclusions

1) The good welded joints without obvious defects can be obtained by EBW for the 8-mm-thick titanium seamless tube. The tensile strength of welded joint is higher than that of base metal, which can reach about 893 MPa. The elongation reaches about 10%, which meets the engineering application standard. The impact energy of FZ reaches ~80% of that of BM, which indicates that the EBW joint achieves a good match of strength and toughness.

2) The coarse β columnar grains are distributed in the FZ, which are composed of Widmanstatten structure, grain boundary α , acicular α' and a small amount of blocky α . With the increase in depth, the acicular α' in FZ becomes finer. The primary HAZ is mainly composed of primary α and acicular α' , and the secondary HAZ mainly consists of lamellar α and acicular α' .

3) The hardness distribution of welded joint is ranked in descending order as FZ, HAZ, and BM. The hardness of HAZ gradually decreases from the location near FZ to the one adjacent to BM side. The bending angles of the bend samples all reach 180° without crack.

References

- 1 Wang T, Yu B, Han K et al. *Journal of Manufacturing Processes*[J], 2019, 45: 147
- 2 Qi Yunlian, Deng Ju, Hong Quan et al. *Materials Science and Engineering A*[J], 2000, 280(1): 177
- 3 Dai J, Zhu J, Chen C et al. *Journal of Alloys and Compounds*[J],

- 2016, 685: 784
- 4 Palanivel R, Dinaharan I, Laubscher R F. *Optik*[J], 2019, 177: 102
 - 5 Su Y, Fan H, You F et al. *Materials Science and Engineering A*[J], 2020, 790: 139 588
 - 6 Warwick J L W, Jones N G, Bantounas I et al. *Acta Materialia*[J], 2013, 61(5): 1603
 - 7 Li W, Chen Z, Liu J et al. *Journal of Materials Science & Technology*[J], 2019, 35(5): 790
 - 8 Yu Z Y, Yu Z T, Liu H Y et al. *Hot Working Technology*[J], 2018, 47(9): 6 (in Chinese)
 - 9 Gao F, Yu W, Song D et al. *Materials Science and Engineering A*[J], 2020, 772: 138 612
 - 10 Sun Z, Karppi R. *Journal of Materials Processing Technology*[J], 1995, 59(3): 257
 - 11 Gao Qi, Jiang Peng, Geng Yongliang et al. *Rare Metal Materials and Engineering*[J], 2020, 49(3): 990 (in Chinese)
 - 12 Su M, Li J, Liu K et al. *Vacuum*[J], 2019, 159: 315
 - 13 Wang S, Lin J, Wen G et al. *Rare Metal Materials and Engineering*, 2013, 42(6): 1150 (in Chinese)
 - 14 Yang X, Li S, Qi H. *Rare Metals*[J], 2016, 35(6): 450
 - 15 Xu Xuefeng, Tayyeb A, Lin W et al. *Journal of Materials Research and Technology*[J], 2020, 9(5): 11 509
 - 16 Ren J, Qi W, Zhang B et al. *Materials Science and Engineering A*[J], 2022, 831: 142 187
 - 17 Wang D, Wang S, Zhang W. *Journal of Engineering Materials and Technology*[J], 2021, 143(2): 21 002
 - 18 Chen J, Wang T, Du Y et al. *Springer Singapore*[C]. Singapore: CMC, 2018: 431
 - 19 Lütjering G. *Materials Science and Engineering A*[J], 1998, 32-45: 921
 - 20 Mohandas T, Banerjee D, Kutumba Rao V V. *Materials Science and Engineering A* [J], 1998, 147-154: 921
 - 21 Suresh N, Pillai M G, Mathew J. *Journal of Materials Processing Technology*[J], 2007, 192-193: 83
 - 22 Zeng L, Bieler T R. *Materials Science and Engineering A*[J], 2005, 392(1-2): 403
 - 23 Lu W, Shi Y, Lei Y et al. *Materials & Design*[J], 2012, 34: 509
 - 24 Li L, Wang S, Huang W et al. *Journal of Manufacturing Processes*[J], 2020, 50: 295
 - 25 Hu J L, Hu Y J, Zeng C Y et al. *Hot Working Technology*[J], 2022, 1-6: 1001 (in Chinese)

热连轧 Ti-Al-Nb-Zr-Mo 系钛合金无缝管电子束焊组织和力学性能

吕雪岩¹, 武少杰^{1,2}, 周晓锋¹, 樊立民¹, 冯靖¹, 程方杰^{1,2}

(1. 天津大学材料科学与工程学院, 天津 300072)

(2. 天津市现代连接技术重点实验室, 天津 300072)

摘要: 采用真空电子束焊接工艺对热连轧成型的 8 mm 厚新型 Ti-Al-Nb-Zr-Mo 系钛合金无缝管进行了环缝焊接试验, 并对焊接接头的微观组织和力学性能进行了测试分析。结果表明, 该无缝管母材基体主要由初生 α 相、 β 转变组织和魏氏组织组成; 焊接接头的熔合区由针状马氏体 α' 相、块状 α 相和魏氏组织组成, 针状马氏体 α' 的尺寸从上至下逐渐减小; 热影响区由初生 α 相和针状马氏体 α' 相组成。焊接接头显微硬度平均值大小依次为: 熔合区>热影响区>母材, 热影响区的显微硬度从近熔合区侧到近母材侧逐渐降低。焊接接头抗拉强度约为 893 MPa, 断裂均发生在母材基体上, 拉伸试样断后伸长率可达 10%。熔合区的冲击功约可以达到母材的 80%, 弯曲试样弯曲角度可以达到 180° 并且无裂纹产生。

关键词: 钛合金; 电子束焊; 微观组织; 力学性能

作者简介: 吕雪岩, 男, 1999 年生, 硕士, 天津大学材料学院, 天津 300072, E-mail: 2020208077@tju.edu.cn